frontiers | Frontiers in Energy Research

TYPE Brief Research Report
PUBLISHED 28 September 2022
DOI 10.3389/fenrg.2022.1002064

OPEN ACCESS

EDITED BY
Marif Daula Siddique,
Virginia Tech, United States

REVIEWED BY
Anwar Shahzad Siddiqui,
Jamia Millia Islamia, India
Amit Kumar,
Thapar Institute of Engineering & Technology, India

*CORRESPONDENCE
Jong Suk Ro,
jongsukro@gmail.com

SPECIALTY SECTION
This article was submitted to Smart Grids,
a section of the journal
Frontiers in Energy Research

RECEIVED 24 July 2022
ACCEPTED 15 August 2022
PUBLISHED 28 September 2022

CITATION
Karn AK, Hameed S, Sarfraz M, Ro JS and Khalid MR (2022), Load shedding for frequency and voltage control in the multimachine system using a heuristic knowledge discovery method.
Front. Energy Res. 10:1002064.
doi: 10.3389/fenrg.2022.1002064

Load shedding for frequency and voltage control in the multimachine system using a heuristic knowledge discovery method

Amrendra Kumar Karn[1], Salman Hameed[1], Mohammad Sarfraz[1], Jong Suk Ro[2,3]* and Mohd Rizwan Khalid[1]

[1]Department of Electrical Engineering, Aligarh Muslim University, Aligarh, India, [2]School of Electrical and Electronics Engineering, Chung-Ang University, Seoul, South Korea, [3]Department of Intelligent Energy and Industry, Chung-Ang University, Seoul, South Korea

The voltage profile of different buses and the rotor dynamics of generators are adversely affected by a generator outage. Generator outages can be minimized using a variety of strategies and algorithms. An AI-based knowledge discovery approach has been reported in this article. This article proposes a technique for identifying sensitive loads and the amount of active and reactive power curtailment for rotor speed regulation and voltage management at the terminals. The MATLAB®/Simulink environment verifies and tests the method's practicality on an IEEE-10-machine-39-bus system. Active power shedding is considered for rotor angle stability, while reactive power is also shedded for maintaining the terminal voltage at the loads. A sequential outage is considered to simulate a scenario where the two generators with the highest active and reactive power are taken out of service. The generator's rotor speed, terminal voltage, and load are measured with and without load restriction. In all situations, the rotor and center of inertia speed are 1 p.u. The average steady-state load terminal voltage is 0.967 V. The average terminal voltage of all load buses improves from 0.933 to 0.972 and 0.936 to 0.971, case-wise. The reported results confirm and validate the effectiveness and applicability of the proposed technique.

KEYWORDS

knowledge discovery, load shedding, multi-machine system, rotor instability, sensitive load, transient performance

1 Introduction

Industry and academic researchers have focused for decades on post-disaster power supply quality. A generator outage is an extreme contingency that might cause network instability. In a centralized context, the load is distributed when a generator leaves the network. The under-frequency condition arises when the active load on the power network hits its limit. Therefore, thermal and capacity ratings are violated in the reactive

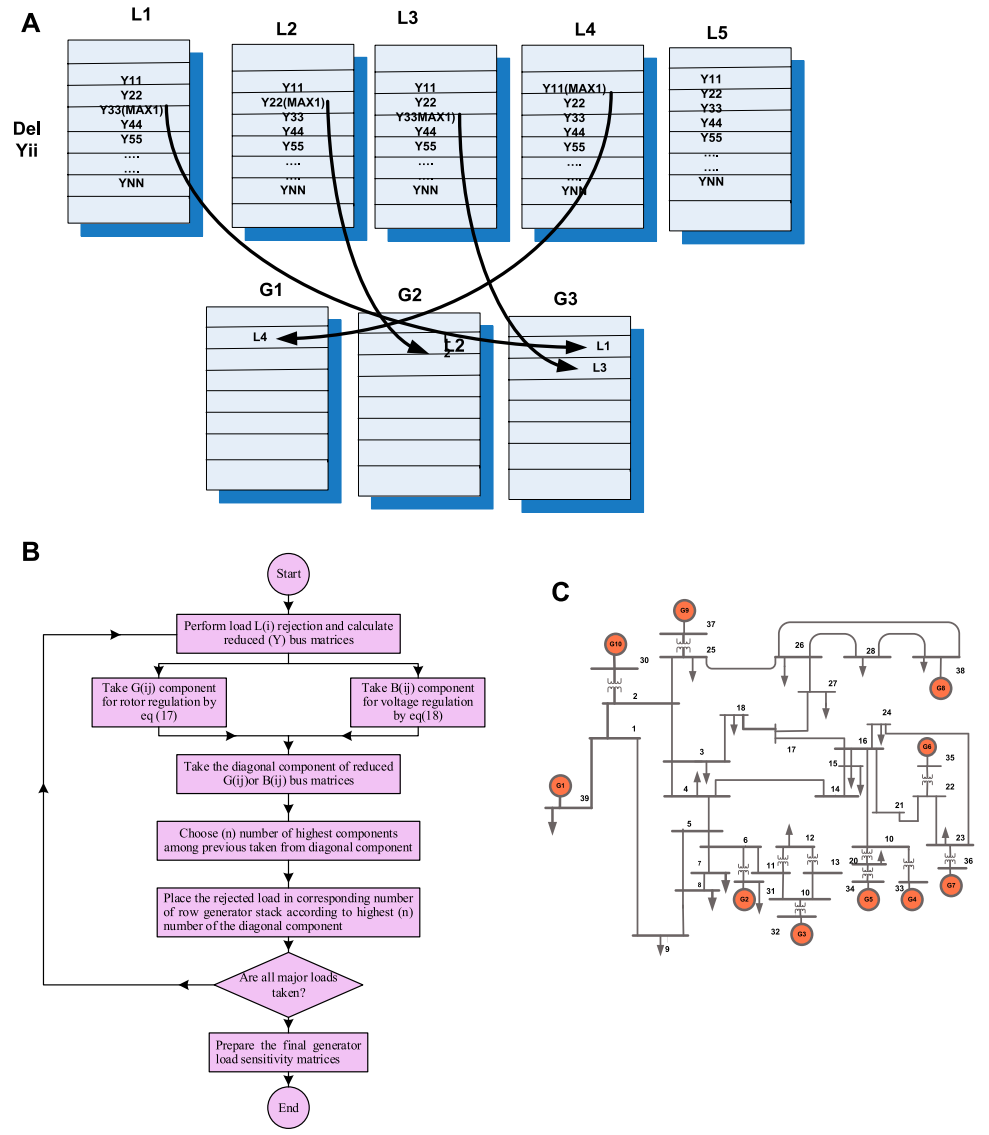

FIGURE 1
(A) Schematic diagram of mapping for knowledge discovery. **(B)** Flow chart of the complete proposed methodology. **(C)** IEEE 39-bus-10-machine system.

load escalation scenario. Active and passive shunt devices exchange active and reactive power to manage active and reactive imbalance through interaction with the existing power network. A power shortfall requires load shedding or curtailing to regulate the system's voltage and frequency. Therefore, load shedding occurs during corrective and emergent power system control. It is recognized that load shedding is a challenging task to ensure power system security. In contrast, in the case of a decentralized environment, there is a tie-line power flow among different control areas.

Recently, researchers are working on load shedding and also on the priority of renewable energy integration in the smart grid. Domestic load shedding is performed in the literature to maintain the supply quality (Azasoo et al., 2020; Alrajhi, 2022), while various sensitivity parameters that combine the negative effects of frequency, voltage, and load shedding are studied through max–min optimization (Alshammari et al., 2018; Alsiraji and El-Shatshat, 2018; Cruz et al., 2020; Talaat et al., 2020; Gharebaghi et al., 2021; Hong and Hsiao, 2022). The authors (Alrajhi, 2018; Jiang et al., 2020) have linearized various components and the system dynamics for load shedding due to the nonlinearity of system voltage dynamics and frequency. An adaptive frequency control-based load frequency control has been

described (Li et al., 2020). The authors (Lin, 2019) use an iterative technique to discover the load shedding. The authors (Alrajhi et al., 2018; Małkowski, 2020; Alrajhi Alsiraji and El-Shatshat, 2021) exhibit adaptive fuzzy load shedding for small power systems. The authors implemented (Nourollah et al., 2019; Nourollah and Gharehpetian, 2019; Potel et al., 2019; Masood et al., 2021) frequency-based multi-topological algorithms. Another study recommended hardening of the electrical system before a cyclone and softening it thereafter to prevent hurricane damage (Sang et al., 2020). Load shedding is implemented by monitoring the active and reactive power delivery and absorption of the synchronous condenser (Sauhats et al., 2021). The author deploys a principle component analysis based on online frequency-measured load shedding (Shi et al., 2019; Skrjanc et al., 2020). A universal load flow-based sensitivity analysis is performed for load shedding to prevent voltage collapse (Tian and Mou, 2019). A secure PV-region mathematical model is developed, and load shedding is conducted (Wang et al., 2020). The authors (Wang et al., 2021) show a dueling deep two-stage Q-learning-based load shedding. The authors (Zhou et al., 2019) provide two-stage load shedding to improve frequency management. LSTM neural network learning-based frequency prediction and load shedding are performed (Zhu and Luo, 2021). Authors (Santos et al., 2019; Deb et al., 2022) use the multi-agent intelligent load shedding method. Authors (Banijamali and Amraee, 2018; Alshammari et al., 2022) describe a method for tripping loads in the case of generator failure.

The state-of-the-art techniques reported in the literature are based on repeating algorithms that account mainly for the generation shortage (Lin, 2019; Jiang et al., 2020; Li et al., 2020; Małkowski, 2020; Masood et al., 2021). During a generation shortage, a load may need to be shedded, but owing to an emergent need, it cannot be scheduled to be disconnected. As a result, to the author's best knowledge, no method or approach in state-of-the-art literature can satisfy this circumstance.

The main contribution of this work is that it describes and implements the heuristic knowledge-based method for load shedding. This study uses active and reactive load deduction in case of generator failure to maintain rotor speed and terminal voltage. The proposed method offers several load-shedding options with precise numerical proportionate rations. The proposed approach has been tested on the IEEE-10-machine-39-bus system.

2 Mathematical background and methodology development

The rotor speed dynamics of the generator in the multi-machine system follow the equation described as follows.

$$\boldsymbol{M}\frac{\boldsymbol{d\omega}}{\boldsymbol{dt}} = \boldsymbol{p_{mi}} - \boldsymbol{p_{ei}} \tag{1}$$

$$p_{ei} = E'_{qi}\left[\sum_{j=1}^{j=n} E'_{qj}\left(B_{ij}\sin\delta_{ij} + G_{ij}\cos\delta_{ij}\right)\right] \tag{2}$$

Substituting Eq. 2 into Eq. 1 and dividing by M lead to obtaining Eq. 3 as follows, where $(\frac{H_i}{\pi f})$ is used in place of M.

$$\frac{d\omega}{dt} = \frac{\left(-E'_{qi}\left[\sum_{j=1}^{j=n} E'_{qj}\left(B_{ij}\sin\delta_{ij} + G_{ij}\cos\delta_{ij}\right)\right] + p_{me}\right)}{\frac{H_i}{\pi f}} \tag{3}$$

In this instance, B_{ij} and G_{ij} are the reduced Y bus matrix, and they can be calculated from the full order matrix of the Y as given in Eq. 4

$$\begin{cases} Y^{BUS} = \overset{GR}{\overbrace{\begin{matrix} G \\ R \end{matrix}\begin{bmatrix} A & B \\ C & D \end{bmatrix}}} \\ Y^{RED} = A - B^{-1}DC \end{cases} \tag{4}$$

Where RED stands for the reduced order bus admittance matrix and the superscript BUS stands for the full order bus admittance matrix. From the Kron reduction formula, this relationship is straightforward to deduce. The admittance matrix elements relating to the generator bus and the remaining other buses, including the load bus, are denoted by the letters G and R, respectively. The sin (ij) and cos (ij) terms in Eq. 3 can be substituted by 0 and 1, respectively, since the impedance angle's change window is very small. Therefore, Eq. 3 can be simplified and written as Eq. 5.

$$\frac{d\omega}{dt} = \frac{\left(-E'_{qi}\left[\sum_{j=1}^{j=n} E'_{qj}G_{ij}\cos\delta_{ij}\right] + p_{me}\right)}{\frac{H_i}{\pi f}} \tag{5}$$

The entire system described by Eqs 6–8 is obtained by expanding Eq. 5 for an n-machine system shown as follows.

$$\frac{d\omega_1}{dt} = \frac{\left(\left[-\left(E'_{q1}2\right)G_{11} - E'_{q1}E'_{q2}G_{12}\cdots - E'_{q1}E'_{qn-1}G_{1n-1} - E'_{q1}E'_{qn}G_{in}\right] + p_{me}\right)}{\frac{H_1}{\pi f}} \tag{6}$$

$$\begin{cases} \Delta\alpha_1 \propto \Delta G_{11} + \Delta G_{12} + \Delta G_{13} \ldots\ldots + \Delta G_{1n} \\ \Delta\alpha_2 \propto \Delta G_{21} + \Delta G_{22} + \Delta G_{23} \ldots\ldots + \Delta G_{2n} \\ \vdots \\ \Delta\alpha_n \propto \Delta G_{n1} + \Delta G_{n2} + \Delta G_{n3} \ldots\ldots + \Delta G_{nn} \end{cases} \tag{7}$$

$$\begin{cases} G_{ii} = \{Y_{i1} + Y_{i2} + Y_{i3} + Y_{i4} + \ldots Y_{in}\} \\ G_{ij} = \{-Y_{ij}\} \end{cases} \tag{8}$$

The value of $\boldsymbol{E'_{q1}}\ldots\ldots\boldsymbol{E'_{qn}}$ varies near about 1p.u. and let $\frac{\boldsymbol{d\omega_1}}{\boldsymbol{dt}} = \boldsymbol{\alpha}$ where $\boldsymbol{\alpha}$ is the angular acceleration

After removal of any load, $\boldsymbol{G_{in}}$ becomes $\boldsymbol{G_{in}} + \boldsymbol{\Delta G_{in}}$. Under balanced condition $\frac{\boldsymbol{d\omega_1}}{\boldsymbol{dt}} = \boldsymbol{\alpha} = 0$. So considering these factors from Eq. 5, a new non-zero $\Delta\,\boldsymbol{\alpha}$ can be approximated as follows

TABLE 1 (A) Load generator sensitivity indexes for rotor speed regulation. (B) Load generator sensitivity indexes for generator voltage regulation.

G1	Sensitivity index (S.I.)	G2	Sensitivity index (S.I.)	G3	Sensitivity index (S.I.)	G4	Sensitivity index (S.I.)	G9	Sensitivity index (S.I.)
L31	92	L6	40	L6	43	L24	271	L39	11,040
L3	91	L24	20	L24	34	L23	240	L29	461
L25	80	L3	18	L15	26	L21	202	L28	259
L24	76	L23	15	L4	26	L12	153	L26	58

G2	Sensitivity index (S.I.)	G3	(Sensitivity index (S.I.)	G4	(Sensitivity index (S.I.)	G5	(Sensitivity index (S.I.)	G6	(Sensitivity index (S.I.)	G10	(Sensitivity index (S.I.)
L8	78	L8	78	L15	72	L20	1860	L4	49	L4	41
L15	24	L4	76	L20	72	L21	32	L8	36	L8	39
No significant data found		L15	37	L21	56	L4	24	No significant data found		No significant data found	

TABLE 2 (A) Active power deduction in case of G_3 outage. (B) Active power deduction in G_9 outage condition. (C) C.O.I steady-state value in different cases.

With proposed methodology			Abrubt way. 1		Abrubt way. 2	
Bus No.	S.I.	MW	Bus No.	MW	Bus No.	MW
L6	43	233	L16	200	L39	650
L24	34	253	L39	300		
L15	26	164	L21	150		

With proposed methodology			With abrupt way. 1		With abrupt way. 2	
Bus No.	S.I.	MW	Bus No.	MW	Bus No.	MW
L39	11,040	775.35	L26	130	L39	830
L29	461	32.37	L27	250		
L28	259	18.19	L28	200		
L26	58	4	L29	250		

Case	C.O.I. speed after 30 s without any outage	C.O.I. speed after 30 s another abrupt load deduction	C.O.I. speed after 30 s with the proposed scheme of load curtailment
G_3 outage	0.9965	0.999	1.0
G_9 outage	0.9955	1.004, 9954	1.0
G_2 and G_3 outage	0.9960	0.9942	1.0

$$\begin{aligned}
\Delta\boldsymbol{\alpha_1} &\underset{\sim}{\propto} \Delta\boldsymbol{G_{11}} + \Delta\boldsymbol{G_{12}} + \Delta\boldsymbol{G_{13}} \ldots\ldots\ldots + \Delta\boldsymbol{G_{1n}} \\
\Delta\boldsymbol{\alpha_2} &\underset{\sim}{\propto} \boldsymbol{G_{21}} + \Delta\boldsymbol{G_{22}} + \Delta\boldsymbol{G_{23}} \ldots\ldots\ldots + \Delta\boldsymbol{G_{2n}} \\
\Delta\boldsymbol{\alpha_3} &\underset{\sim}{\propto} \Delta\boldsymbol{G_{31}} + \Delta\boldsymbol{G_{32}} + \Delta\boldsymbol{G_{33}} \ldots\ldots\ldots + \Delta\boldsymbol{G_{3n}} \\
&\vdots \\
\Delta\boldsymbol{\alpha_n} &\underset{\sim}{\propto} \Delta\boldsymbol{G_{n1}} + \Delta\boldsymbol{G_{n2}} + \Delta\boldsymbol{G_{n3}} \ldots\ldots\ldots + \Delta\boldsymbol{G_{nn}}
\end{aligned} \tag{9}$$

Here, $\underset{\sim}{\propto}$ is the symbol of proportionality. Since

TABLE 3 (A) Reactive power delivery by generators in case of generator outage and with active power deduction. (B) Active and reactive power deduction in case of G_3 Outage. (C) Active and reactive power deduction in a different way in G6 outage. (D) Load voltage in G_3 outage condition with different load sheddings. (E) Load voltage in G_6 outage condition with different load sheddings.

Generator	Normal reactive power dispatch	Reactive power case, G3 outage with proposed active power deduction	Reactive power case, G6 outage with proposed active power deduction
G1	275.5	309.1	304.5
G2	197.7	243.9	208.7
G3	195.6	xxxx	207.9
G4	150.6	162.8	158.1
G5	136.4	141.6	141.2
G6	146.4	159.7	157.4
G7	150.8	156.1	156.6
G8	34.19	41.26	128.2
G9	66.21	71.35	Xxxxx
G10	96.58	118.4	84.02

With proposed method					With abrubt METHOD.1			With abrubt METHOD.2		
BUS	S.I.	MW	BUS	MVR	BUS	MW	MVR	BUS	MW	MVR
L6	43	233	L8 78	80	L4	200	100	L39	650	196.4
L24	34	253	L4 76	78	L3	200	Not applicable			

With proposed method					With abrupt METHOD.1			With abrubt METHOD.2		
BUS	MW	MVR			BUS	MW	MVR	BUS	MW	MVR
L 4	350	110	L4	400	150			L39	650	190
L8	300	80	L27	250	40.6					

Load end	Normal voltage	G3 outage condition	Load shedding with proposed method	Load shedding from L4, L8, and L3	Load shedding from L39
L3	0.9626	0.9241	0.9636	0.9738	0.984
L4	0.94	0.8975	0.9461	0.9567	0.9673
L6	0.9483	0.9076	0.9514	0.9602	0.969
L8	0.9427	0.9046	0.9503	0.9593	0.9683
L15	0.9447	0.9031	0.9621	0.9508	0.9395
L16	0.9598	0.922	0.9581	0.9655	0.9729
L18	0.9615	0.9237	0.9717	0.9705	0.9693
L21	0.9582	0.9236	0.9661	0.9627	0.9593
L23	0.9732	0.9412	0.9953	0.9762	0.9571
L24	0.9649	0.9277	0.9861	0.9703	0.9545
L25	0.995	0.9679	0.9698	1.003	1.0362
L26	0.9863	0.9538	0.9875	0.9937	0.9999
L27	0.9695	0.9348	0.971	0.9769	0.9828
L28	0.9884	0.9586	0.9894	0.9955	1.0016
L29	0.9905	0.9623	0.9914	0.9975	1.0036

(Continued on following page)

TABLE 3 (*Continued*) (A) Reactive power delivery by generators in case of generator outage and with active power deduction. (B) Active and reactive power deduction in case of G_3 Outage. (C) Active and reactive power deduction in a different way in G6 outage. (D) Load voltage in G_3 outage condition with different load sheddings. (E) Load voltage in G_6 outage condition with different load sheddings.

With proposed method			With abrupt METHOD.1			With abrubt METHOD.2		
BUS	**MW**	**MVR**	**BUS**	**MW**	**MVR**	**BUS**	**MW**	**MVR**
L39	0.9982	0.9756	0.9967			1.005		1.0133
Average terminal voltage	0.9677375	0.93300625	0.9722875			0.9761		0.9799125

Load end	Normal voltage	G6 outage condition	Load shedding with the proposed method from L4 and L8	Load shedding from L39	Load shedding from L4 and L27
L3	0.9626	0.9334	0.971	0.9456	0.9752
L4	0.94	0.9126	0.9546	0.9233	0.9635
L6	0.9483	0.9218	0.9589	0.9346	0.9605
L8	0.9427	0.9155	0.954	0.931	0.9542
L15	0.9447	0.9137	0.949	0.9163	0.9539
L16	0.9598	0.9263	0.959	0.9261	0.9656
L18	0.9615	0.9307	0.9702	0.9366	0.9722
L21	0.9582	0.9188	0.957	0.9165	0.9576
L23	0.9732	0.9288	0.967	0.922	0.9671
L24	0.9649	0.9308	0.97	0.9299	0.9703
L25	0.995	0.9663	0.998	0.978	1.001
L26	0.9863	0.9539	0.989	0.96	0.9955
L27	0.9695	0.9367	0.973	0.9414	0.983
L28	0.9884	0.9575	0.989	0.9624	0.9933
L29	0.9905	0.9604	0.991	0.9652	0.9941
L39	0.9982	0.9707	0.994	0.975	0.999
Average termnal voltage	0.9677375	0.93611875	0.97154375	0.94149375	0.975375

$$\boldsymbol{G_{ii}} = \{\boldsymbol{Y_{i1}} + \boldsymbol{Y_{i2}} + \boldsymbol{Y_{i3}} + \boldsymbol{Y_{i4}} + \ldots \boldsymbol{Y_{in}}\} \text{ and } \boldsymbol{G_{ij}} = \{-\boldsymbol{Y_{ij}}\} \quad (10)$$

So $|\Delta \boldsymbol{G_{ii}}|'' \gg |\Delta \boldsymbol{G_{ij}}|$ So again

$$\Delta \boldsymbol{\alpha_i} \underset{\sim}{\propto} \Delta \boldsymbol{G_{ii}} \quad (11)$$

So the $\Delta \boldsymbol{\alpha_i}$ reflection can be easily seen in $\boldsymbol{G_{ii}}$

Now quadrature axis terminal voltage follows the dynamics of the equation as follows

$$\dot{\boldsymbol{E}}_{\boldsymbol{qi}}^{'} = \left[-\left(\boldsymbol{E}_{\boldsymbol{qi}}^{'} + (\boldsymbol{x_{di}} - \boldsymbol{x}_{\boldsymbol{di}}^{'})\boldsymbol{I_{di}}\right) + \boldsymbol{E_{fi}} \right] \Big/ \boldsymbol{T_{doi}} \quad (12)$$

$$\dot{E}_{qi}^{'} = \left[-\left(E_{qi}^{'} + (x_{di} - x_{di}^{'}) \sum_{j=1}^{j=n} E_{qj}^{'} \left(G_{ij} \sin \delta_{ij} - B_{ij} \cos \delta_{ij} \right) \right) + E_{fi} \right] \Big/ T_{doi} \quad (13)$$

Again angle $\boldsymbol{\delta_{ij}} = [\mathbf{0}\ \mathbf{5}]$ so $\sin \boldsymbol{\delta_{ij}}$ can be substituted by 0 and $\cos \boldsymbol{\delta_{ij}}$ can be substituted by 1. After remodifying Eq. 13, we get Eq. 14

$$\dot{E}_{qi}^{'} = \left[-\left(E_{qi}^{'} + (x_{di} - x_{di}^{'}) \sum_{j=1}^{j=n} E_{qj}^{'} B_{ij} \right) + E_{fi} \right] \Big/ T_{doi} \quad (14)$$

Again taking perturbation terms

$$\dot{E}_{qi}^{'} + \Delta \dot{E}_{qi}^{'} = \left[-\left(E_{qi}^{'} + \Delta E_{qi}^{'} + (x_{di} - x_{di}^{'}) \sum_{j=1}^{j=n} \Delta E_{qj}^{'} B_{ij} + (x_{di} - x_{di}^{'}) \sum_{j=1}^{j=n} E_{qj}^{'} \Delta B_{ij} \right) + E_{fi} \right] \Big/ T_{doi} \quad (15)$$

By substituting Eq. 12 from Eq. 13

$$\dot{E}_{qi}^{'} + \Delta \dot{E}_{qi}^{'} = \left[-\left(E_{qi}^{'} + \Delta E_{qi}^{'} + (x_{di} - x_{di}^{'}) \sum_{j=1}^{j=n} \Delta E_{qj}^{'} B_{ij} + (x_{di} - x_{di}^{'}) \sum_{j=1}^{j=n} E_{qj}^{'} \Delta B_{ij} \right) + E_{fi} \right] \Big/ T_{doi} \quad (16)$$

$$\Delta \dot{\boldsymbol{E}}_{\boldsymbol{qi}}^{'} \underset{\sim}{\propto} (\boldsymbol{x_{di}} - \boldsymbol{x}_{\boldsymbol{di}}^{'}) \sum_{\boldsymbol{j=1}}^{\boldsymbol{j=n}} \boldsymbol{E}_{\boldsymbol{qj}}^{'} \Delta \boldsymbol{B_{ij}} \quad (17)$$

$$\Delta \dot{\boldsymbol{E}}_{\boldsymbol{q1}}^{'} \underset{\sim}{\propto} (\boldsymbol{x_{di}} - \boldsymbol{x}_{\boldsymbol{di}}^{'}) [\Delta \boldsymbol{B_{11}} + \Delta \boldsymbol{B_{12}} + \Delta \boldsymbol{B_{13}} \ldots\ldots + \Delta \boldsymbol{B_{1n}}] \quad (18)$$

Again $\Delta E_{qi}^{'} = 0$ because $\Delta E_{qi}^{'}$ is instantaneous change, and instantaneous change in voltage is always zero due to inductance of the circuit, and there is no control performance so ΔE_{fi} term does not appear. So putting $\Delta E_{qi}^{'}$ term = 0. The final equation with proportional approximation can be obtained as follows and assuming that $E_{qj}^{'} = 1, \forall j \in \mathbb{N}[1 \ldots n]$

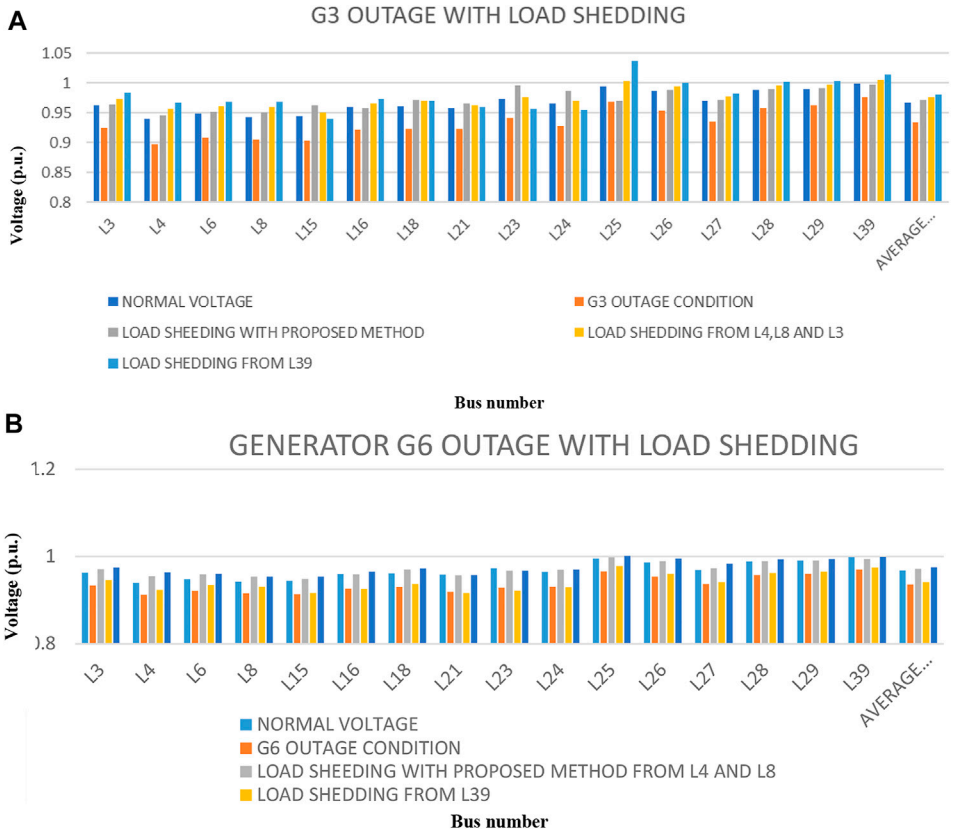

FIGURE 2
(A) Voltage profile of load terminal in case of generator G_3 outage with different manners of load shedding. **(B)** Voltage profile of load terminal in case of generator G_6 outage with different manners of load shedding.

$$\Delta E'^{\alpha}_{q'\sim}(x_{di}-x_{di})\sum_{j=1}^{j=n}E'_{qj}\Delta B_{ij}$$
$$E'^{\alpha}_{q'\sim}\left(x_{di}-x'_{di}\right)[\Delta B_{11}+\Delta B_{12}+\Delta B_{13}\ldots\ldots+\Delta B_{1n}] \quad (19)$$

Since again $\Delta B_{ii} = -[\Delta B_{i1} + \Delta B_{i2} + \Delta B_{i3} + \ldots\ldots\ldots\ldots \Delta B_{in}]$

So $|\Delta B_{ii}| \gg "|\Delta B_{ij}|"$

Neglecting the ΔB_{ij} due to very smaller in magnitude than ΔB_{ii}.So according to the aforesaid explanations and assumption

$$\begin{aligned}\Delta \dot{E}'_{q1} &= (x_{di}-x'_{di})\Delta B_{11}\\ \Delta \dot{E}'_{q2} &= (x_{di}-x'_{di})\Delta B_{22}\\ &\vdots\\ \Delta \dot{E}'_{qn} &= (x_{di}-x'_{di})\Delta B_{nn}\end{aligned} \quad (20)$$

3 Methodology

This article uses a rotor and voltage terminal paradigm to collect the information. The data are collected by rejecting the loads in a one-by-one fashion. The changes in load-rejection admittance matrices can be sampled. Later, loads for a particular generator are picked using inductive logic from rotor dynamics and machine voltage. The heuristic knowledge base has three levels, namely, 1) database creation/variable declaration, 2) finding the variable relationships by performing a preset database operation, and 3) systematically using the proposed knowledge-based technique.

3.1 Database creation using variables

Changes in conductance and susceptance cause variations in the rotor speed and the generator terminal voltage, as given in Eqs 6, 16. The load is eliminated in the simulation background, and the changes in conductance and susceptance are retained in a folder with the load as a heading. Repeat until all loads are coated. The subject variables considered are loads, and the object variables are generators.

3.1.1 Knowledge retrieval by identifying variable relationships through database operations

Load L_a is removed, and the diagonal elements G_{ii} and B_{ii} from Eqs 6, 16 are maintained in a separate block (2), as shown in Figure 1A. Higher values G_{ii} and B_{ii} are selected and maintained in

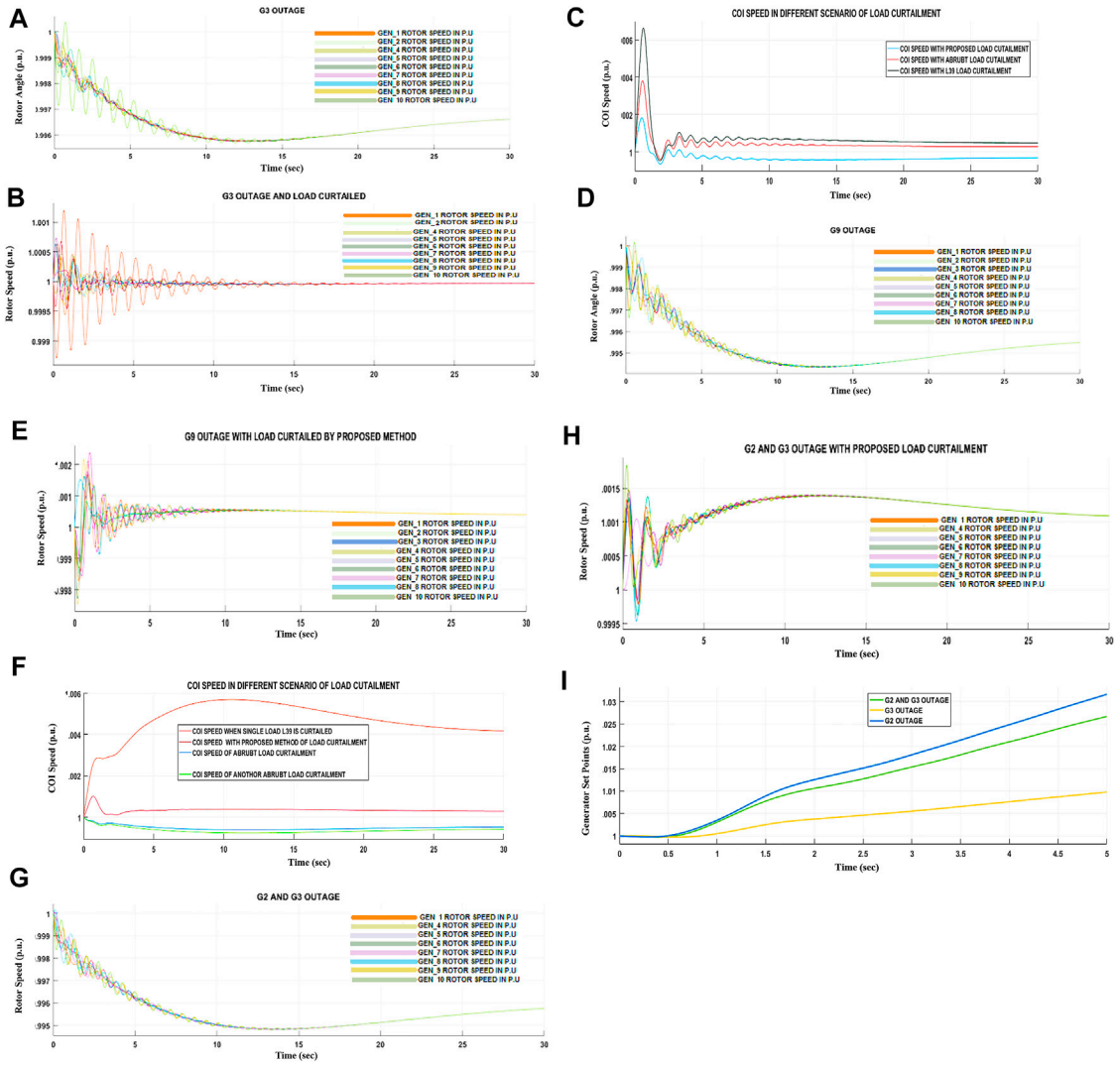

FIGURE 3
(A) Rotor speed of generator in case of G3 outage. **(B)** Rotor speed of generator in case of G_3 outage with proposed load shedding. **(C)** Center of inertia speed of generator in case of G_3 outage scenario in different combination load shedding. **(D)** Rotor speed of generator in case of G_9 outage. **(E)** Rotor speed of generator in case of G_9 outage with proposed load shedding. **(F)** Center of inertia speed of generator in G_9 outage scenario in different combinations of load shedding. **(G)** Rotor speed of generator in case of G_2 and G_3 outage. **(H)** Rotor speed of generator in case of G_2 and G_3 outage with proposed load shedding. **(I)** Generator set point variation of G_1 in simulation environment.

the generator group G (*i*) block. Repeat until all significant active and reactive loads are removed. The mapping operation with the actual data set is presented in Figure 1A. The final generator load sensitivity (S_1) is represented in Table 1A. Tables 1A, B summarize generator load sensitivity for speed regulation and voltage regulation, respectively. The complete algorithm is shown in Figure 1B.

3.1.2 Deployment of proposed technique in load shedding

In the case of any particular generator outage of capacity P_{GEN}, it is found that three loads, L_a, L_b, and L_c have the highest sensitivity index with values w_{La}, w_{Lb}, and w_{Lc}. Then curtailment of power C_{La}, C_{Lb}, and C_{Lc} is defined as:

$$C_{La} = (P_{GEN}{}^{*}w_{La})/((w_{La} + w_{Lb} + w_{Lc}))$$
$$C_{Lb} = (P_{GEN}{}^{*}w_{Lb})/((w_{La} + w_{Lb} + w_{Lc}))$$
$$C_{Lc} = (P_{GEN}{}^{*}w_{Lc})/((w_{La} + w_{Lb} + w_{Lc})).$$

If any of C_{La}, C_{Lb}, or C_{Lc} is greater than the installed capacity of a load L_a, L_b, and L_c, then that particular load is separated, and the remaining power is curtailed from other remaining loads.

TABLE 4 Reactive power delivery and generator terminal voltage under all conditions of generator G_3 outage.

GEN NO.	MVR ** A	MVR**B	MVR **C	MVR **D	MVR**E	VOL*A	VOL*B	VOL*C	VOL*D	VOL*E
G1	275.5	309.1	267.4	251.6	234.7	0.9988	1	0.9974	0.987	1.008
G2	197.7	243.9	183.1	169.9	260.6	0.9995	1	0.9965	0.987	1.01
G3	195.6	XXX	XXX	XXX	XXX	0.9981	XXX	XXX	XXX	XXX
G4	150.6	162.8	148.1	156.6	159.4	0.9989	0.999	0.9961	0.9868	1.01
G5	136.4	141.6	134.8	137	142	0.9989	0.999	0.996	0.9863	1.01
G6	146.4	159.7	143.5	152.8	156.9	0.9986	0.999	0.995	0.9864	1.01
G7	150.8	156.1	148.8	157.1	153.3	0.9991	0.999	0.9963	0.987	1.01
G8	34.19	41.26	29.49	31.62	57.93	0.9982	0.999	0.9953	0.9857	1.01
G9	66.21	71.35	66.48	74.72	68.96	0.9989	0.999	0.9966	0.987	1.009
G10	96.58	118.4	101.2	94.09	108.1	0.9987	0.999	0.9967	0.9865	1.009
Average						0.99877	0.999222	0.996211	0.986633	1.009556

*A normal condition without any generator outage. *B G3 outage with only active power deduction with proposed methodology. *C G3 outage with active and reactive both power deduction with proposed methodology. *D G3 outage with active and reactive both power deduction in abrupt way. *E G3 outage with active and reactive both power deduction with another abrupt way.

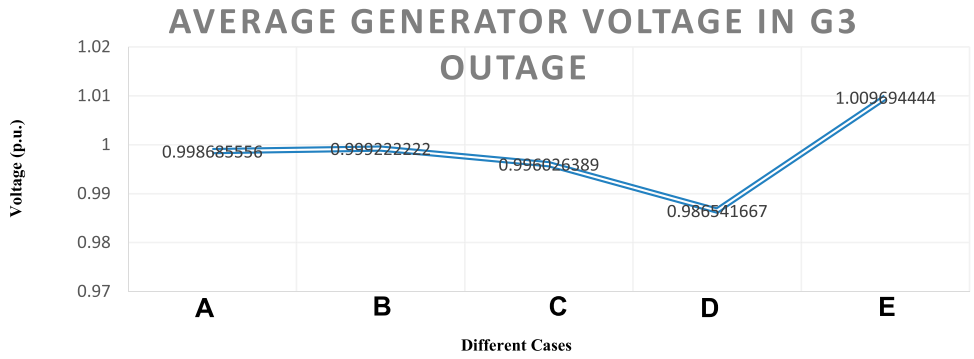

FIGURE 4
Average voltage of remaining generators in case of G_3 outage in all Cases.

The load generator sensitivity indexes, shown in Tables 1A, B, are prepared with four loads assigned with their priority in the target set for generators G_1, G_2, G_3, G_4, and G_5 for the concern of rotor stability. Table 1B is prepared for load terminal voltage according to Eq. 16. Each generator delivers active and reactive power to the network to meet the load demand.

4 Results and discussion

The proposed method is applied to a 10-machine-IEEE-39-bus system in the MATLAB®/Simulink environment. It includes 10 different-sized generators G_1 ... G_{10} and 19 loads L_a, L_b, and L_c. Here, *a*, *b*, and *c* are the bus numbers where the load is situated. The total capacity of the system is 61,408 MW, and the total load is 60,936 MW. The individual generator capacities of G_1 to G10 are [1,000,520.81, 650,632, 508,650, 560,540, 830,250] MW. All generators have voltage regulators, speed governors, and power system stabilizers. Any generator outage changes the generator's rotor speed and terminal voltage.

4.1 Case of generator outage with only active power curtailment

In this section, only active power is deducted from the sensitive load to regulate the speed of the remaining generators and reactive power dispatch. Initially, generator G_3 of capacity 650 MW and G9 of capacity 830 MW are taken out one-by-one, further, generators G_2 and G_3 are taken out.

The center of inertia is expressed as $\omega_{coi} = \frac{\sum_{i=1}^{i=n} \omega_i H_i}{\sum_{i=1}^{i=n} H_i}$. The center of interia speed reflects the total system speed. Tables 2A, B show the different load curtailments performed under the G_3 and G_9 outages. In tables, the first column summarizes the sensitivity index The different cases are shown in Figure 3.

4.2 Both active and reactive power deduction

As discussed in sections #2 and #3 for the terminal voltage regulation scenario, generator G_3 in the first case and generator G_6 in the second case are subjected to the outage. As discussed in Section 3, for voltage profile maintenance, the reactive power should be shedded. In the generator G_3 outage case, power is deducted according to Table 3B, and in the case of G_6 outage, power deduction is carried out according to Table 3C. All the load voltages after power deduction are mentioned in Tables 3D, E and also bar charts in Figures 2A,B.

5 Conclusion

In this article, a heuristic knowledge-based load shedding method is proposed. The load generator sensitivity matrices are assembled as the final process of knowledge discovery to provide the amount and location of power to be curtailed in case of a generator outage. The proposed methodology described in this article is applied to three generator outage cases, and the results are shown as a deviation of the center of inertia speed, as in Figure 3C. It is found that the proposed method of load shedding gives a C.O.I speed of 1 p.u while deducting only the active power, but the reactive power is more stressed on generators according to Table 3A. In contrast, if both active and reactive power is deducted using the proposed method, the load voltage is closer to normal than the other abrupt methods. Finally, the generator G_3 outage condition is examined in detail, as summarized in Table 4 and Figure 4. It is concluded that the proposed method is more cost-effective in reactive power management and voltage conditions.

Data availability statement

The original contributions presented in the study are included in the article/Supplementary Material; further inquiries can be directed to the corresponding author.

Author contributions

All authors listed have made a substantial, direct, and intellectual contribution to the work and approved it for publication.

Funding

This work was supported by the National Research Foundation of Korea (NRF) grant funded by the Korea government (MSIT) (No. NRF-2022R1A2C2004874). This work was supported by the Korea Institute of Energy Technology Evaluation and Planning (KETEP) and the Ministry of Trade, Industry and Energy (MOTIE) of South Korea (No. 20214000000280).

Conflict of interest

The authors declare that the research was conducted in the absence of any commercial or financial relationships that could be construed as a potential conflict of interest.

Publisher's note

References

Alrajhi, A. H. (2018). A new virtual synchronous machine control structure for voltage source converter in high voltage direct current applications. *umm al qura Univ. J. Eng. Archit. X* 33, 1–6.

Alrajhi Alsiraji, H., and El-Shatshat, R. (2021). Virtual synchronous machine/dual-droop controller for parallel interlinking converters in hybrid AC–DC microgrids. *Arab. J. Sci. Eng.* 46, 983–1000. doi:10.1007/s13369-020-04794-y

Alrajhi, H. (2022). A generalized state space average model for parallel dc-to-dc converters. *Comput. Syst. Sci. Eng.* 41 (2), 717–734. doi:10.32604/csse.2022.021279

Alshammari, K., Alrajhi, H., and El-Shatshat, R. (2022). Optimal power flow for hybrid AC/MTDC systems. *Arab. J. Sci. Eng.* 47, 2977–2986. doi:10.1007/s13369-021-05983-z

Alshammari, K., Alsiraji, H. A., and Shatshat, R. E., (2018), "Optimal power flow in multi -terminal HVDC systems," 2018 IEEE Electrical Power and Energy Conference (EPEC), 10-11 October 2018, Toronto, ON, Canada, pp. 1–6. doi:10.1109/EPEC.2018.8598298

Alsiraji, H. A., and El-Shatshat, R. (2018). "Serious operation issues and challenges related to multiple interlinking converters interfacing a hybrid AC/DC microgrid," in 2018 IEEE Canadian Conference on Electrical & Computer Engineering (CCECE), Quebec, QC, Canada, 13-16 May 2018, 1–5. doi:10.1109/CCECE.2018.8447831

Alsiraji, H. (2018). "Operational control and analysis of a hybrid AC/DC microgrid,". Ph.DAdvisor (Hybrid, AC, and DC Microgrids: UWSpace). Available at: http://hdl.handle.net/10012/13053.

Azasoo, J. Q., Kanakis, T, Al-Sherbaz, A, and Michael Opoku Agyeman (2020). Heuristic optimization for microload shedding in generation constrained power systems. *IEEE Access* 8, 13294–13304. doi:10.1109/ACCESS.2020.2965819

Banijamali, S. S., and Amraee, T (2018). Semi-adaptive setting of under frequency load shedding relays considering credible generation outage scenarios. *IEEE Trans. Power Deliv.* 34 (3), 1098–1108. doi:10.1109/tpwrd.2018.2884089

Cruz, L M., Alvarez, D L., Al-Sumaiti, A S., and Rivera, S (2020). Load curtailment optimization using the PSO algorithm for enhancing the reliability of distribution networks. *Energies* 13, 3236–3312. doi:10.3390/en13123236

Deb, S., Al Ammar, E. A., AlRaihi, H., Alsaidan, I., and Shariff, S. M. (2022). *V2G pilot projects: Review and lessons learnt", developing charging infrastructure and technologies for electric vehicles*. Pennsylvania, United States: IGI-Global, 252–267.

Gharebaghi, S., Vennelaganti, S. G., Chaudhuri, N. R., Ting, H., Thomas, F., and La Porta (2021). Inclusion of pre-existing undervoltage load shedding schemes in AC-QSS cascading failure models. *IEEE Trans. Power Syst.* 36 (6), 5645–5656. doi:10.1109/TPWRS.2021.3075210

Hong, Y Y, and Hsiao, C Y (2022). Under-frequency load shedding in a standalone power system with wind-turbine generators using fuzzy PSO. *IEEE Trans. Power Deliv.* 37 (2), 1140–1150. doi:10.1109/TPWRD.2021.3077668

Jiang, M, Guo, Q, Sun, H, and Ge, H (2020). Decoupled piecewise linear power flow and its application to under voltage load shedding. *CSEE J. Power Energy Syst.* 7 (5), 976–985. doi:10.17775/CSEEJPES.2019.02900

Li, C, Wu, Y, Sun, Y, Zhang, H, Liu, Y, Liu, Y, et al. (2020). Continuous under-frequency load shedding scheme for power system Adaptive frequency control. *IEEE Trans. Power Syst.* 35 (2), 950–961. doi:10.1109/TPWRS.2019.2943150

Lin, F. (2019). Worst-case load shedding in electric power networks. *IEEE Trans. Control Netw. Syst.* 6 (3), 1269–1277. doi:10.1109/TCNS.2019.2935559

Małkowski, R. (2020). Małkowski, Nieznański_2020_Underfrequency load shedding an innovative algorithm based on fuzzy logic. *Energies* 13, 1456. doi:10.3390/en13061456

Masood, N-A., Shazon, M. N. H., Rahman Deeba, S., and Modak, S. R. (2021). A frequency and voltage stability-based load shedding technique for low inertia power systems. *IEEE Access* 9, 78947–78961. doi:10.1109/ACCESS.2021.3084457

Nourollah, S., Aminifar, F., and Gharehpetian, G. B. (2019). A hierarchical regionalization-based load shedding plan to recover frequency and voltage in microgrid. *IEEE Trans. Smart Grid* 10 (4), 3818–3827. doi:10.1109/TSG.2018.2837160

Nourollah, S., and Gharehpetian, Gevork B. (2019). Coordinated load shedding strategy to restore voltage and frequency of microgrid to secure region. *IEEE Trans. Smart Grid* 10 (4), 4360–4368. doi:10.1109/TSG.2018.2857840

Potel, Barnabé, Vincent, Debusschere, Cadoux, Florent, and Urban, Rudez (2019). A real-time adjustment of conventional under-frequency load shedding thresholds. *IEEE Trans. Power Deliv.* 34 (6), 2272–2274. doi:10.1109/TPWRD.2019.2900594

Sang, Yuanrui, Xue, Jiayue, Sahraei-Ardakani, Mostafa, and Ou, Ge (2020). An integrated preventive operation framework for power systems during hurricanes. *IEEE Syst. J.* 14 (3), 3245–3255. doi:10.1109/JSYST.2019.2947672

Santos, Athila Quaresma, Machado Monaro, Renato, Coury, Denis Vinicius, and Oleskovicz, Mario (2019). A new real-time multi-agent system for under frequency load shedding in a smart grid context. *Electr. Power Syst. Res.* 174, 105851. doi:10.1016/j.epsr.2019.04.029

Sauhats, Antans, Utans, Andrejs, Silinevics, Jurijs, Junghans, Gatis, and Guzs, Dmitrijs (2021). Enhancing power system frequency with a novel load shedding method including monitoring of synchronous condensers' power injections. *Energies* 14, 1490–1495. doi:10.3390/en14051490

Shi, Fang, Zhang, Hengxu, Cao, Yongji, Sun, Huadong, and Chai, Yun (2019). Enhancing event-driven load shedding by corrective switching with transient security and overload constraints. *IEEE Access* 7, 101355–101365. doi:10.1109/ACCESS.2019.2929304

Skrjanc, T., Mihalic, R., and Rudez, U. (2020). Principal component analysis (PCA)-Supported underfrequency load shedding algorithm. *Energies* 13 (22), 5896. doi:10.3390/en13225896

Talaat, M., Hatata, A. Y., Alsayyari, Abdulaziz S., and Alblawi, Adel (2020). A smart load management system based on the grasshopper optimization algorithm using the under-frequency load shedding approach. *Energy* 190, 116423. ISSN 0360-5442. doi:10.1016/j.energy.2019.116423

Tian, A., and Mou, X. (2019). A network analysis-based distributed load shedding strategy for voltage collapse prevention. *IEEE Access* 7, 161375–161384. doi:10.1109/ACCESS.2019.2950628

Wang, C., Mei, S., Dong, Q., Chen, R., and Zhu, B. (2020). Coordinated load shedding control scheme for recovering frequency in islanded microgrids. *IEEE Access* 8, 215388–215398. doi:10.1109/ACCESS.2020.3041273

Wang, C., Yu, H., Chai, Lin, Liu, H., and Zhu, B. (2021). Emergency load shedding strategy for microgrids based on dueling Deep Q-learning. *IEEE Access* 9, 19707–19715. doi:10.1109/ACCESS.2021.3055401

Zhou, Q., Li, Z., Wu, Q., and Shahidehpour, M. (2019). Two-stage load shedding for secondary control in hierarchical operation of islanded microgrids. *IEEE Trans. Smart Grid* 10 (3), 3103–3111. doi:10.1109/TSG.2018.2817738

Zhu, L., and Luo, Y. (2021). Deep feedback learning based predictive control for power system undervoltage load shedding. *IEEE Trans. Power Syst.* 36, 4 3349–3361. doi:10.1109/TPWRS.2020.3048681

10.3389/fenrg.2022.1002064

Nomenclature

E'_{qi} sub transient quadrature axis of the stator

E_{fi} rotor field voltage reference

G_{ij} conductance of reduced bus matrices between bus

B_{ij} susceptance of reduced bus matrices between bus

δ_{ij} angle difference between buses

x_{di} direct axis reactance of the generator

x'_{di} sub transient direct axis reactance of the generator

T_{doi} the open axis time constant of the rotor field circuit

$\Delta E'_{qi}$ an instantaneous change in sub transient quadrature axis voltage of the stator

ΔE_{fi} an instantaneous change in the rotor field

ΔB_{ij} an instantaneous change in susceptance of reduced bus matrices between buses

$\Delta\ G_{ij}$ an instantaneous change in conductance of reduced bus matrices between buses

$G(i)$ generator number

$L(i)$ load situated at bus i